Mineralogical Magazine (2025), **89**, 242–249
doi:10.1180/mgm.2024.82

CAMBRIDGE UNIVERSITY PRESS

Article

Ferrodimolybdenite, $FeMo^{3+}{}_2S_4$ from Daba-Siwaqa, Jordan – the first natural compound of trivalent molybdenum

Evgeny V. Galuskin[1], Irina O. Galuskina[1], Joachim Kusz[2], Maria Książek[2], Yevgeny Vapnik[3] and Grzegorz Zieliński[4]

[1]Institute of Earth Sciences, Faculty of Natural Sciences, University of Silesia, Będzińska 60, 41-200 Sosnowiec, Poland; [2]Faculty of Science and Technology, University of Silesia, ul. 75. Pułku Piechoty 1, 41-500 Chorzów, Poland; [3]Department of Geological and Environmental Sciences, Ben-Gurion University of the Negev, P.O.B. 653, Beer-Sheva 84105, Israel; and [4]Polish Geological Institute – National Research Institute, Rakowiecka 4, 00-975 Warsaw, Poland

Abstract

Ferrodimolybdenite with ideal formula $FeMo^{3+}{}_2S_4$ (*C*2/*c*, $a = 11.8249(8)$ Å, $b = 6.5534(3)$ Å, $c = 13.0052(10)$ Å, $\beta = 114.474(9)°$, $V = 917.27(12)$ Å^3 and $Z = 8$) was discovered in a differentiated sulfide nodule composed of troilite and pentlandite parts. The nodule was detected in the central zone of a diopside–anorthite–tridymite oval paralava body, ~30 metres in diameter, within the pyrometamorphic Hatrurim Complex in Daba-Siwaqa, Jordan. Ferrodimolybdenite is the first trivalent molybdenum compound discovered in Nature. Its synthetic analogue crystallises in the *C*1*c*1 space group. Ferrodimolybdenite with the empirical formula $(Fe^{2+}{}_{0.99}Cu^{2+}{}_{0.07}Ni^{2+}{}_{0.04})_{\Sigma 1.10}Mo^{3+}{}_{1.94}(S^{2-}{}_{3.98}P^{3-}{}_{0.02})_{\Sigma 4.00}$ was identified in the troilite part of the differentiated sulfide nodule. The nodule contains inclusions of tetrataenite, nickelphosphide, molybdenite, galena and rudashevskyite. Ferrodimolybdenite forms platy crystals with dimensions ranging from 3×100 μm to 20×40 μm. The mineral exhibits a grey colour and a dark grey streak. It is opaque with a metallic lustre, and its Mohs hardness is ~3. The cleavage observed in the mineral is perfect on {001}, good on {100} and poor on {010}. Its tenacity is sectile, and its fracture is smooth. The calculated density of 5.445 g·cm^{-3} was derived from the empirical formula and unit cell volume refined from single-crystal X-ray diffraction data. In reflected light, ferrodimolybdenite appears grey to light grey with a blueish tinge. It is anisotropic, with a reflectance in the range of 34–40%. The crystallisation of ferrodimolybdenite occurred in reduced conditions in monosulfide Fe(+Ni) melt at a temperature of 1000–1100°C and at low pressure.

Keywords: new mineral; ferrodimolybdenite; crystal structure; Mo^{3+}; Daba-Siwaqa; Jordan; Hatrurim Complex

(Received 4 September 2024; accepted 13 October 2024; Accepted Manuscript published online: 11 November 2024)

Introduction

Ferrodimolybdenite, $FeMo^{3+}{}_2S_4$ (*C*2/*c*, $a = 11.8249(8)$ Å, $b = 6.5534(3)$ Å, $c = 13.0052(10)$ Å, $\beta = 114.474(9)°$, $V = 917.27(12)$ Å^3 and $Z = 8$) was identified in a sulfide nodule (~7 mm) in the central part of an oval diopside–anorthite–tridymite paralava body with a diameter of ~30 m within a field of spurrite-bearing rocks of the Hatrurim Complex, Daba-Siwaqa, Jordan. This paralava is the site of the first description of 11 new phosphides and phosphates, which were found to be concentrated along the contact between the paralava and host altered sedimentary rocks (Britvin *et al.*, 2015; Galuskin *et al.*, 2025). The mineral composition and conditions of paralava formation, as well as the genetic aspects of phosphide and phosphate crystallisation in this paralava, are considered elsewhere (Galuskin *et al.*, 2023a, 2025).

Ferrodimolybdenite is the first natural compound of trivalent molybdenum. All known minerals contain molybdenum in an oxidation state of +4 or +6; however, molybdenum can be found in a reduced form in phosphides (Murashko *et al.*, 2022). A metallic Mo, hexamolybdenum, has been identified in the Allende meteorite (Ma *et al.*, 2014). It has previously been determined that the synthetic compound $FeMo^{3+}{}_2S_4$ belongs to the *C*1*c*1 space group ($a = 11.8148(2)$ Å, $b = 6.5499(1)$ Å, $c = 13.014(2)$ Å, $\beta = 114.455(1)°$ and $V = 916.75$ Å^3) (Guillevic *et al.*, 1974; Vaqueiro *et al.*, 2002), whereas for ferrodimolybdenite we have accepted a model with the *C*2/*c* space group.

The present article provides a description of a new mineral, ferrodimolybdenite, $FeMo^{3+}{}_2S_4$. The mineral and name have been approved by the Commission on New Minerals, Nomenclature and Classification (CNMNC) of the International Mineralogical Association (IMA), IMA2023–019 (mineral symbol – Fdmol). The mineral name ferrodimolybdenite is derived from its composition

Corresponding author: Evgeny V. Galuskin; Email: evgeny.galuskin@us.edu.pl
Associate Editor: Peter Leverett
Cite this article: Galuskin E.V., Galuskina I.O., Kusz J., Książek M., Vapnik Y. and Zieliński G. (2025) Ferrodimolybdenite, $FeMo^{3+}{}_2S_4$ from Daba-Siwaqa, Jordan – the first natural compound of trivalent molybdenum. *Mineralogical Magazine* **89**, 242–249. https://doi.org/10.1180/mgm.2024.82

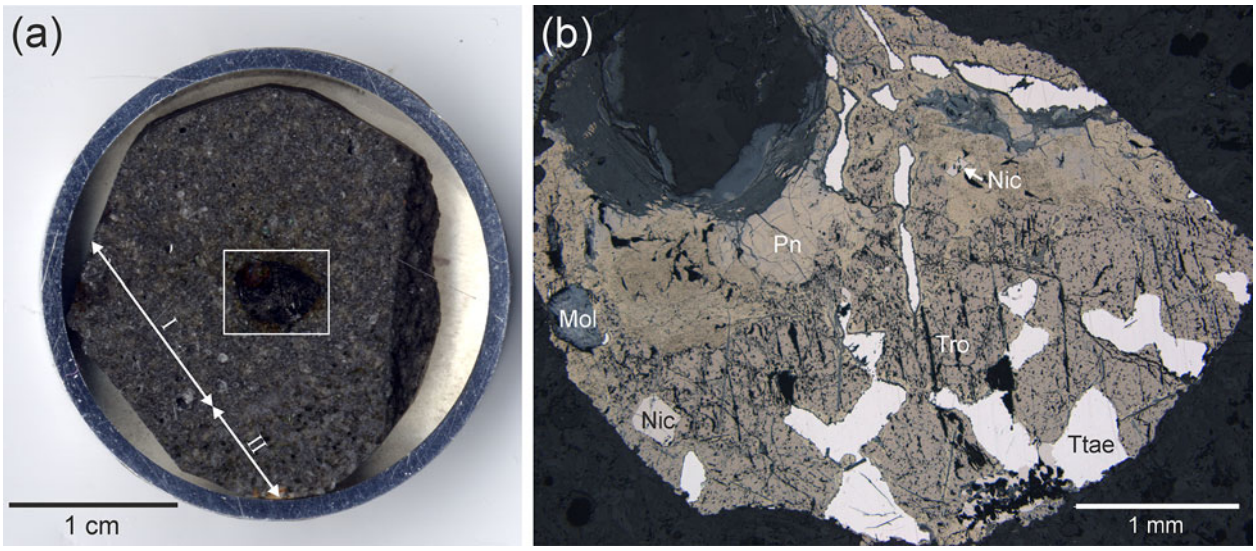

Figure 1. (a) Sulfide nodules in diopside–anorthite–tridymite paralava. I - porous rock and II - massive rock. The fragment outlined (holotype specimen 6005/1) is enlarged in Fig. 1b. (b) Reflected light image of the differentiated sulfide nodule with a gas bubble (upper part) and composed of troilite and pentlandite zones. Relatively large inclusions of tetrataenite and nickelphosphide are present in the troilite zone. Tro = troilite; Ttae = tetrataenite; Mol = molybdenite; Pn = pentlandite and Nic = nickelphosphide [Mineral symbols here and below according to Warr (2021)].

and structure: 'ferro' refers to Fe^{2+}, whereas 'di+molybdenite' indicates the presence of two MoS_2 layers. Type material has been deposited in the mineralogical collection of the Fersman Mineralogical Museum, Leninskiy pr., 18/k. 2, 115162 Moscow, Russia, registration number: 6005/1.

Methods of investigation

The morphology and composition of ferrodimolybdenite and associated minerals were studied using optical microscopy, scanning electron microscopes (Phenom XL and Quanta 250, Institute of Earth Sciences, Faculty of Natural Sciences, University of Silesia, Sosnowiec, Poland) and an electron microprobe analyser (Cameca SX100, Micro-Area Analysis Laboratory, Polish Geological Institute – National Research Institute, Warsaw, Poland). Chemical analyses of sulfide nodule minerals were conducted in WDS mode (wavelength-dispersive spectroscopy, settings: 15 kV, 20 nA and ~1 μm beam diameter) using the following lines and standards: Mo*Lβ* – Mo; Cu*Kα* – Cu; Ni*Kα* – pentlandite; Fe*Kα* – FeS_2; S*Kα* – FeS_2, ZnS; P*Kα* – InP; Si*Kα*, Mg*Kα* – diopside; Al*Kα* – orthoclase; Se*Lβ* – In_2Se_3; As*Lβ*, Co*Kα* – $CoNiAs_3$; Ca*Kα* – apatite; Sb*Lα* – Sb_2Te_3; Pb*Mβ* – pyromorphite; Zn*Kα* – ZnS; Mn*Kα* – rhodonite; Cr*Kα* – Cr_2O_3; V*Kα* – V; and Ti*Kα* – rutile. Other chemical elements were below the detection limit.

The Raman spectra of ferrodimolybdenite and molybdenite were recorded on a WITec alpha 300R Confocal Raman Microscope (Department of Earth Science, University of Silesia, Poland) equipped with an air-cooled solid laser (488 nm) and a CCD camera operating at –61°C. The laser radiation was coupled to a microscope through a single-mode optical fibre with a diameter of 3.5 μm. An air Zeiss LD EC Epiplan-Neofluan DIC-100/0.75NA objective was used. The Raman scattered light was focused onto a multi-mode fibre and monochromator with a 1800 gr mm^{-1} grating. The laser power at the sample position was 5–7 mW. Twenty scans with an integration time of 3 s and a resolution of 2 cm^{-1} were collected and averaged. The spectrometer monochromator was calibrated using the Raman scattering line of a silicon plate (520.7 cm^{-1}).

Single-crystal X-ray diffraction (XRD) studies of ferrodimolybdenite were carried out using a SuperNova diffractometer with a mirror monochromator (Mo*Kα* and $\lambda = 0.71073$ Å) and an Atlas CCD detector (formerly Agilent Technologies, currently Rigaku Oxford Diffraction) at the Institute of Physics, University of Silesia, Poland. Single-crystal XRD data were collected using a ferrodimolybdenite crystal fragment 40×30×10 μm in size. The ferrodimolybdenite structure was refined using the *SHELX-2019/2* program (Sheldrick, 2015). The crystal structure was refined starting from the atomic coordinates of synthetic $FeMo_2S_4$ (Vaqueiro *et al.*, 2002).

Background information

The pyrometamorphic rocks of the Hatrurim Complex, represented by spurrite, larnite and gehlenite rocks, form large fields along the Dead Sea Rift in Israel, Palestine and Jordan. Descriptions of the Hatrurim Complex can be found in numerous publications (Bentor, 1960; Gross, 1977; Vapnik *et al.*, 2007; Geller *et al.*, 2012; Novikov *et al.*, 2013; Khoury *et al.*, 2014; Galuskina *et al.*, 2014). The genesis of the Complex remains an unsolved problem, but all researchers agree that the rocks of the Hatrurim Complex are products of combustion metamorphism. Two genetic hypotheses have been proposed, the first of which relates pyrometamorphic transformations of the sedimentary protolith to the combustion of dispersed organic fuels (Kolodny and Gross, 1974; Matthews and Gross, 1980; Geller *et al.*, 2012). The second hypothesis suggests that fires were activated by methane combustion originating from the tectonically active Dead Sea rift zone (Sokol *et al.*, 2010; Novikov *et al.*, 2013). Locally, melting of rocks of the protolith of the Hatrurim Complex can be observed, along with the formation of paralavas and slag-like rocks of different composition, forming bodies of different sizes from thin veins, ranging from gehlenite hornfels with a thickness of a few centimetres to large oval fields of diopside-bearing paralava with a diameter of

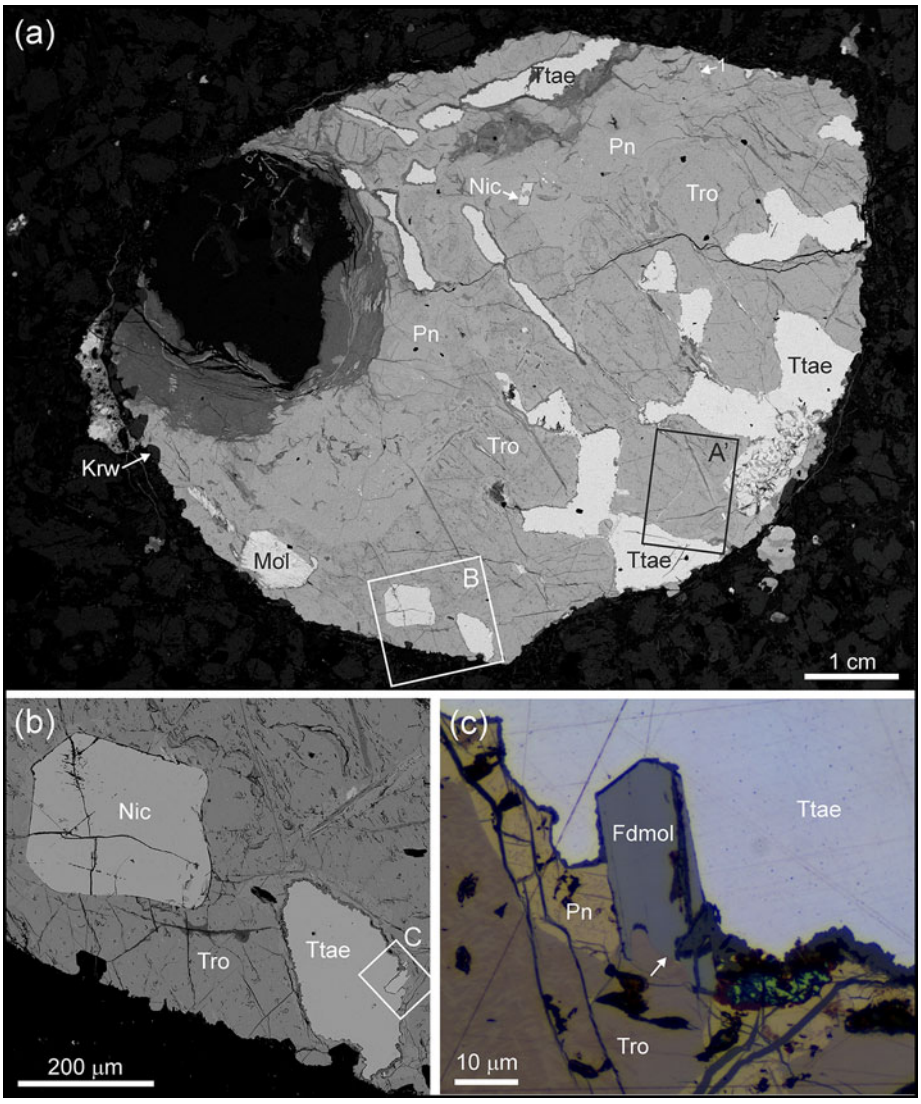

Figure 2. (a) Back-scattered electron (BSE) images of a sulfide nodule in which ferrodimolybdenite was discovered. The areas outlined are magnified in: Fig. 2b ('B') and Fig. 3a ('A'). (b) BSE image of nickelphosphide and tetrataenite inclusions in troilite. The frame ('C') outlines the area magnified in Fig. 2c. (c) Reflected light image of the ferrodimolybdenite crystal has a inductive growth surface with troilite (arrow, simultaneous growth) and idiomorphism with respect to pentlandite and tetrataenite. Fdmol = ferrodimolybdenite; Krw = karwowskiite; Mol = molybdenite; Nic = nickelphosphide; Pn = pentlandite; Tro = troilite; and Ttae = tetrataenite.

tens of metres. The near-surface character of the paralava generation processes determines the predominantly oxidised mineral composition of the paralavas, with minerals containing only Fe^{3+} (Galuskina *et al.*, 2017). In relatively rare cases, black reduced paralavas enriched with pyrrhotite are formed. The rarest are paralavas containing native iron and phosphides, as well as osbornite – an indicator of super-reduced conditions (Btitvin *et al.*, 2015; Galuskin *et al.*, 2022, 2023b, 2025; Futrzyński *et al.*, 2023). The hypothesis of phosphide and native iron formation as a result of reducing carbothermal reactions occurring at the boundary of hot paralava and thermally altered sedimentary rock enriched with graphitised and phosphoritised organic residues has been proposed elsewhere (Galuskin *et al.*, 2022, 2023b, 2025). One of the rare examples of a reduced paralava is from Daba-Siwaqa, Jordan. Along with numerous aggregates of phosphides in the contact facies, this paralava features a sulfide nodule with inclusions of tetrataenite and nickelphosphide, containing ferrodimolybdenite crystals. It was found in the central part of the body (Galuskin *et al.*, 2025).

Occurrence and composition

Ferrodimolybdenite was found in a small quarry (prospecting for phosphorite deposits) in the Daba-Siwaqa complex within the Transjordan Plateau, Jordan (31°22'01"N, 36°11'10"E), where a basalt-like paralava body ~30 metres in diameter is exposed in pyrometamorphically altered carbonate rocks of the Muwaqqar Chalk-Marl Formation. The paralava consists of diopside, anorthite, wollastonite, tridymite and small amounts of glass. Cristobalite is observed growing on tridymite crystals (Trd), exhibiting specific cracking patterns reminiscent of fish scales, indicative of the transition $Trd_{cub} \rightarrow Trd_{tetr}$ and a paralava generation temperature exceeding 1400°C (Galuskin *et al.*, 2023a). Fluorapatite, titanite and spinel of the

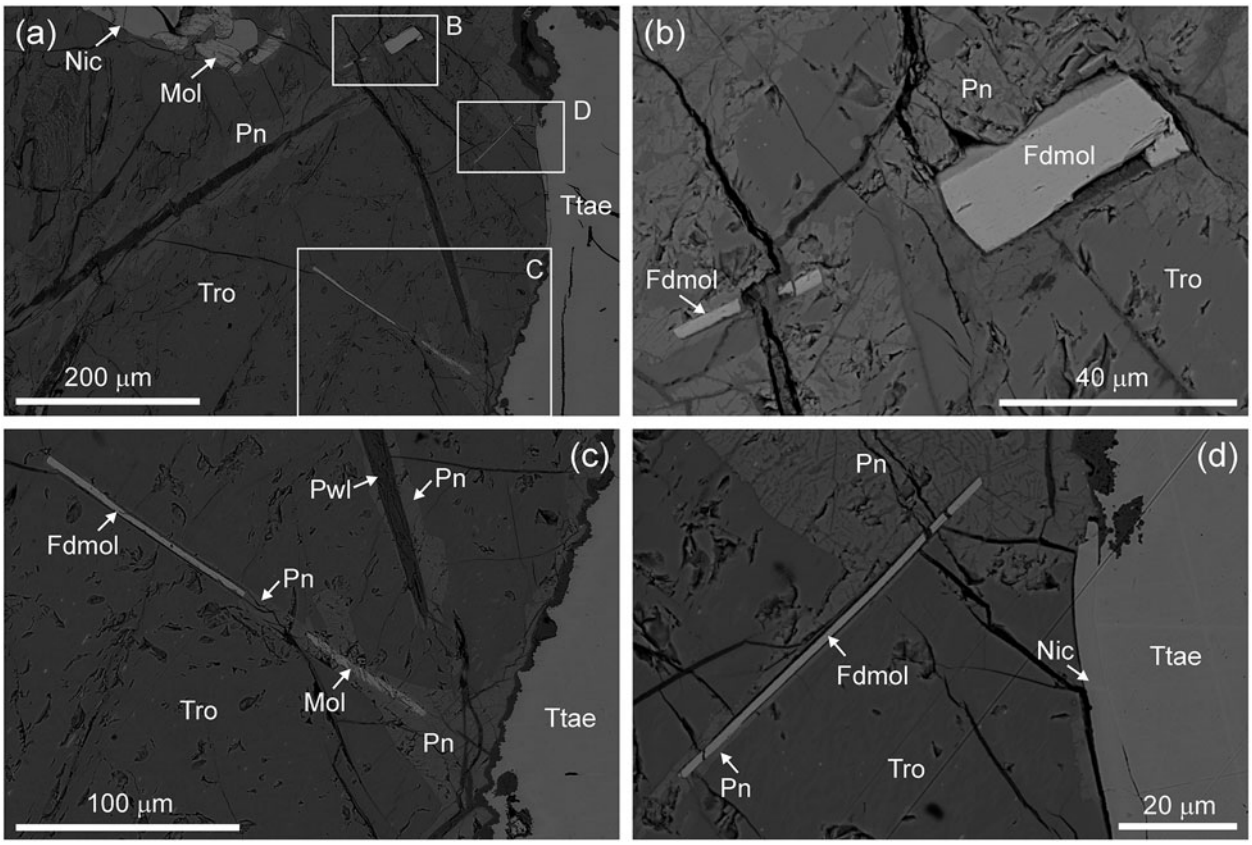

Figure 3. BSE images. (a) Fragment of sulfide nodule (from Fig. 2a) with ferrodimolybdenite crystals. The frames outline the areas magnified in Fig. 3b–d, respectively. (b) Relatively large ferrodimolybdenite crystal used for the single-crystal XRD study. (c, d) Fine lamellar crystals of ferrodimolybdenite (cross-section is ~ parallel to Z), usually with a thin film of pentlandite. Tro = troilite; Ttae = tetrataenite; Mol = molybdenite; Pn = pentlandite; Nic = nickelphosphide; Fdmol = ferrodimolybdenite; and Pwl = powellite.

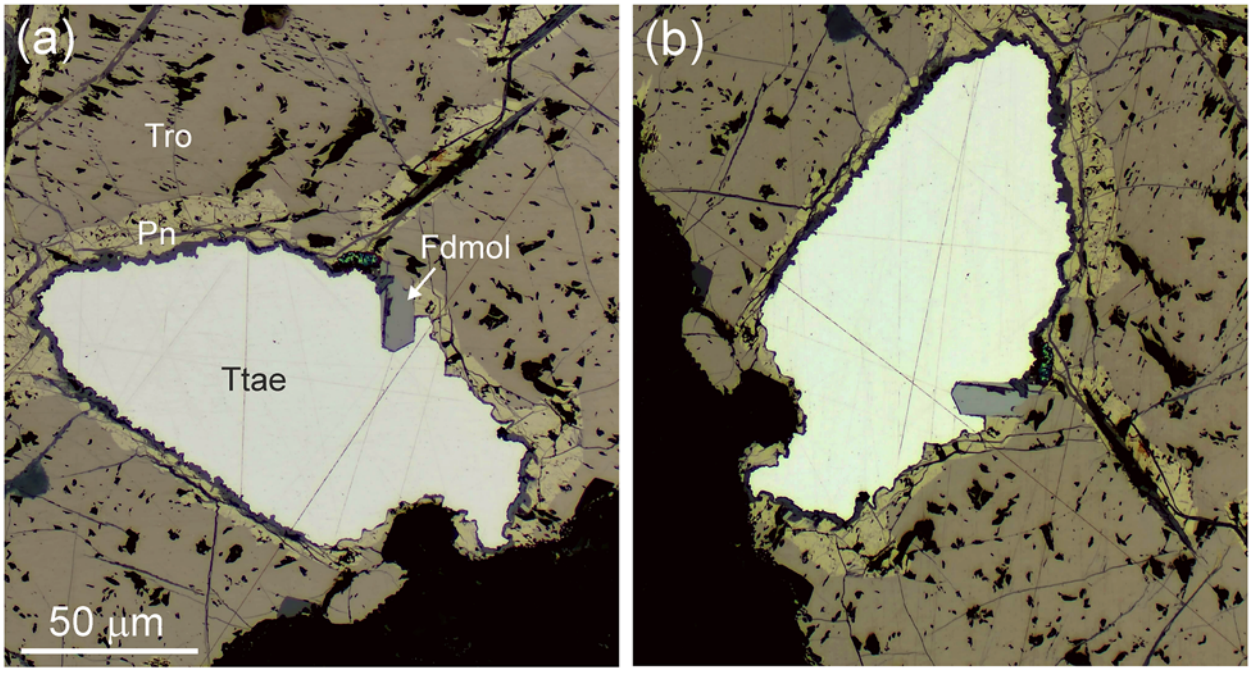

Figure 4. Ferrodimolybdenite (centre right) in reflected light is (a) grey to light-grey with (b) a bluish tinge; the mineral exhibits strong bireflectance. This crystal is also shown, magnified, in Fig. 2c. Tro = troilite; Ttae = tetrataenite; Pn = pentlandite; and Fdmol = ferrodimolybdenite.

Table 1. Reflectivity of ferrodimolybdenite*

R_{max}	R_{min}	λ (nm)	R_{max}	R_{min}	λ (nm)
35.7	34.2	400	36.9	35.1	560
35.8	34.3	420	37.1	35.7	580
35.9	34.3	440	37.3	35.9	**589**
36.0	34.4	460	37.8	36.0	600
36.0	34.4	**470**	38.2	36.2	620
36.1	34.4	480	38.9	36.8	640
36.2	34.4	500	39.0	37.0	**650**
36.3	34.5	520	39.2	37.2	660
35.5	34.9	540	39.8	37.8	680
36.7	35.0	**546**	40.0	38.1	700

* The values required by the Commission on Ore Mineralogy (COM) are given in bold.

Table 2. Chemical composition (wt.%) of ferrodimolybdenite

Constituent	~~n~~	S.D.	Range
Mo	49.30	0.39	48.96–49.95
Cu	1.19	0.19	0.92–1.43
Ni	0.58	0.14	0.39–0.77
Fe	14.64	0.22	14.31–14.93
S	33.90	0.14	33.69–34.03
P	0.15	0.01	0.15–0.17
Total	99.78		

n = number of spot analyses; S.D. = standard deviation.

magnesioferrite–magnetite–chromite series are the accessory minerals of the paralava. Ferrodimolybdenite was identified in a sulfide nodule ~7 mm in size (Fig. 1) found in the central part of the paralava body (Galuskin *et al.*, 2025). The sulfide nodule comprises troilite and pentlandite zones and gaseous bubbles (Figs 1b, 2a). Inclusions of tetrataenite, nickelphosphide, molybdenite, (rarely) galena and rudashevskyite are observed. The presence of crystals of the new mineral karwowskiite, with a composition of $Ca_9Mg(Fe^{2+}_{0.5}\square_{0.5})(PO_4)_7$ (IMA2023–080), was detected on the boundary between the nodule and the paralava (Galuskin *et al.*, 2024). These crystals were absent in the groundmass of the rock. An analysis of the nodule minerals is presented in Galuskin *et al.* (2025). The composition of tetrataenite varies in the range $Fe_{0.59}Ni_{0.39}Cu_{0.01}$ – $Ni_{0.53}Fe_{0.44}Cu_{0.02}$ with a tendency for the Ni content to increase towards the edge of the grain. The composition of nickelphosphide also varies significantly, so the smallest crystals are characterised by the highest Ni content (up to 2.57 Ni per formula unit), while in the relatively large crystals in the centre the Ni content decreases to 2.06 Ni pfu, with a tendency to increase towards the edge of the crystal.

Ferrodimolybdenite forms separate tabular crystals in a sulfide matrix, with dimensions ranging from 3 μm to 20 μm in the cross-section (Figs 2c, 3, 4). Ferrodimolybdenite crystals are typically found in the troilite zone, with a thin pentlandite film commonly observed between ferrodimolybdenite and troilite (Fig. 3b–d). Ferrodimolybdenite is grey in colour with a dark grey streak. The mineral is opaque with a metallic lustre. Its Mohs hardness is ~3. Ferrodimolybdenite crystals show cleavage in three directions: perfect on {001}, good on {100} and poor on {010}. Its tenacity is sectile, and its fracture is smooth. Its density, 5.445 g·cm^{-3}, was calculated from the empirical formula and unit cell volume refined from the single-crystal XRD data. The mineral is slightly magnetic. In reflected light, it is grey to light grey with a bluish tinge. It is strongly anisotropic (Fig. 4). No internal reflections have been observed. The reflectivity varies between 34.2% and 40.0% (Table 1).

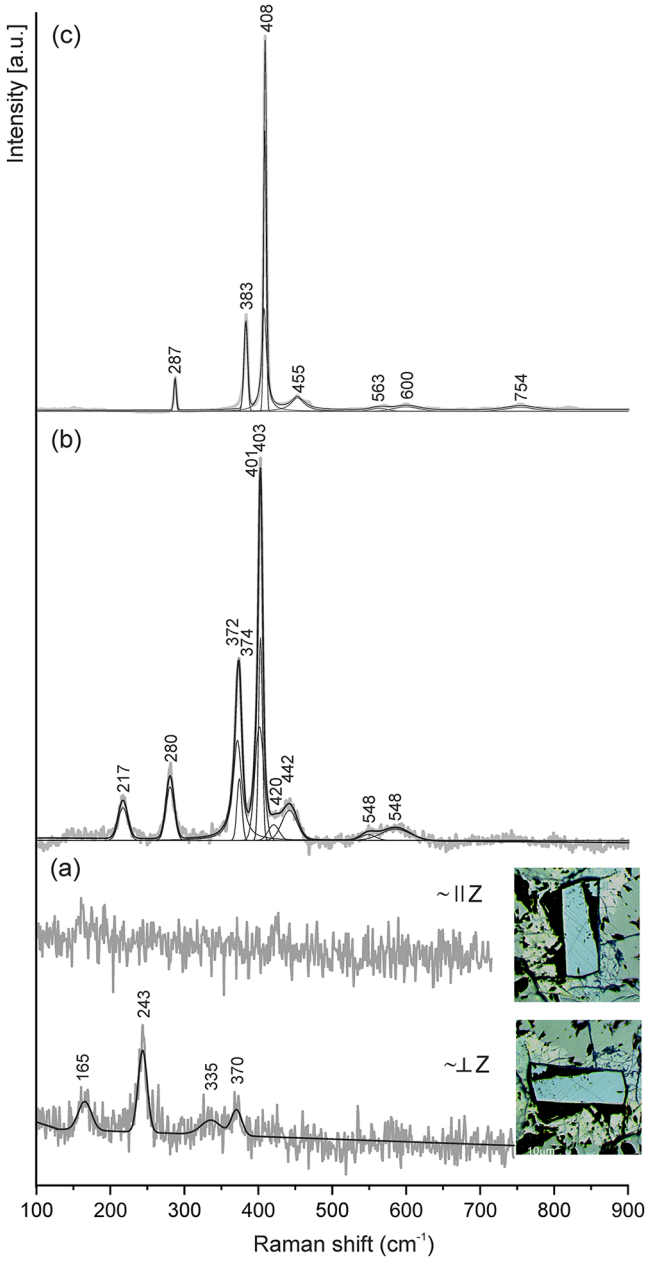

Figure 5. (a) Raman spectra of ferrodimolybdenite; crystal orientation during the measurements is shown. (b) Raman spectrum of thermally altered ferrodimolybdenite. (c) Raman spectrum of molybdenite from the sulfide nodule.

The chemical composition of ferrodimolybdenite is close to stoichiometric $(Fe^{2+}_{0.99}Cu^{2+}_{0.07}Ni^{2+}_{0.04})_{\Sigma 1.10}Mo^{3+}_{1.94}(S^{2-}_{3.98}P^{3-}_{0.02})_{\Sigma 4.00}$ (Table 2). The simplified formula of ferrodimolybdenite is $(Fe^{2+},Cu^{2+},Ni^{2+})Mo_2S_4$, leading to the ideal formula $FeMo_2S_4$. Interestingly, a 3 μm grain of the Cu-analogue of ferrodimolybdenite, with the composition $(Cu_{0.78}Fe_{0.22})Mo_2S_{\sim 4}$ was found in the inclusion in the tetrataenite.

Raman spectroscopy

In the Raman spectrum of ferrodimolybdenite at laser beam polarisation (~ ⊥ *Z*, ~ parallel to molybdenite layers), a single weak

Table 3. Parameters for X-ray data collection and crystal-structure refinement for ferrodimolybdenite

Crystal data		**Refinement of structure**	
Formula from refinement	$Fe^{2+}Mo^{3+}{}_2S_4$	Reflection measured	6695
Crystal system	Monoclinic	No. of unique reflections	2133
Space group	*C*2/*c* (no. 15)	No. of observed unique refl. [$I>3\sigma(I)$]	1619
Unit-cell dimensions		Refined parameters	64
a (Å)	11.8249(8)	*Rint*	0.0376
b (Å)	6.5534(9)	R_1/R_{all}	0.0297/0.0469
c (Å)	13.0052(10)	w*R*	0.0569
β (°)	114.474	Goof	1.034
V (Å^3)	917.27(12)	Δρmin (*e* Å^{-3})	−1.563
Z	8	Δρmax (*e* Å^{-3})	2.201
Crystal size (mm)	0.040×0.030×0.010		
Data collection			
Diffractometer	SuperNova with Atlas CCD	Weighting scheme	$w = 1/[\sigma^2(F_O{}^2) + (0.0207P)^2]$
Radiation wavelength	Mo*K*a, λ = 0.71073 Å		
Min. & max. theta (°)	3.44, 36.16		
Reflection ranges	$-19 \le h \le 17$		
	$-10 \le k \le 10$		
	$-19 \le l \le 21$		

Table 4. Atom coordinates (*x*,*y*,*z*), equivalent isotropic displacement parameters (U_{eq}, Å^2) for ferrodimolybdenite

Site	Atom	*x*	*y*	*z*	U_{eq}
Mo1	Mo	0.09969(2)	0.39854(5)	−0.00541(2)	0.00574(8)
Mo2	Mo	−0.09122(2)	0.14863(5)	0.00741(2)	0.00592(8)
Fe1	Fe	0.25958(4)	0.37567(11)	0.25116(4)	0.01127(15)
S1	S	0.03565(7)	0.38106(14)	0.14654(7)	0.00712(16)
S2	S	0.24706(7)	0.37973(14)	−0.10464(7)	0.00703(16)
S3	S	0.26566(7)	0.63228(14)	0.11266(7)	0.00699(16)
S4	S	−0.01610(7)	0.12869(14)	−0.13516(7)	0.00715(16)

band at 243 cm^{-1} related to the stretching Mo–S vibration is observed (Fig. 5a). When laser beam power is increased, a dark spot appears on the surface of ferrodimolybdenite in which the Raman spectrum corresponds to that of molybdenite (Fig. 5b,c).

Crystal structure

Single-crystal XRD and refinement showed the cation and anion sites are fully occupied. Details of data collection and structure refinement are given in Table 3, final atomic coordinates are summarized in Table 4, and anisotropic displacement parameters are given in Table 5. Selected bond lengths and bond valence sum (BVS) calculations are given in Table 6. The crystallographic information file has been deposited with the Principal Editor of *Mineralogical Magazine* and is available as Supplementary material (see below).

Ferrodimolybdenite (*C*2/*c*; $a = 11.8249(8)$ Å, $b = 6.5534(3)$ Å, $c = 13.0052(10)$ Å, $\beta = 114.474(9)°$ and $V = 917.27(12)$ Å^3), like its synthetic analogue (*C*1*c*1; $a = 11.8148(2)$ Å, $b = 6.5499(1)$ Å, $c = 13.014(2)$ Å, $\beta = 114.455(1)°$ and $V = 916.75$ Å^3) (Guillevic *et al.*, 1974; Vaqueiro *et al.*, 2002), crystallises with monoclinic symmetry and has a structure formed by layers of octahedra $\infty(MoS_2)^-$ with columns of Fe^{2+}-octahedra between them (Fig. 6a). Ferrodimolybdenite has a centrosymmetric structure, two types of Mo-octahedra and one type of Fe-octahedra (Fig. 6a,b). In the synthetic analogue there is no inversion centre and a reduction in symmetry is illustrated by the presence of four types of Mo-octahedra and two types of Fe-octahedra. The ferrodimolybdenite structure can be considered a molybdenite structure, where molybdenite layers are divided by parallel columns of Fe-octahedra. In natural molybdenite the $\infty(MoS_2)^0$ layers consist of trigonal prisms $(MoS_6)^{8-}$, not octahedra. Distorted octahedra have only been found in synthetic molybdenite–1T Mo (Samy *et al.*, 2021). Mo-bearing sulfides with the general formula AMo_2S_4 (*A* = V, Cr, Fe and Co) are isostructural with Cr_3S_4 (space group *C*2/*m*). In this space group, the symmetry only allows distortions involving the formation of zigzag cation chains (Vaqueiro *et al.*, 2002). A reduction in symmetry from *C*2/*m* (archetype of the Cr_3S_4 structure) to *C*1*c*1 for artificial $FeMo_2S_4$ can be related both to its synthesis conditions (Canadell *et al.*, 1988) and to the deformation of its crystals during pulverisation for powder diffraction.

Table 5. Anisotropic displacement parameters (Å^2) for ferrodimolybdenite

Site	U^{11}	U^{22}	U^{33}	U^{12}	U^{13}	U^{23}
Mo1	0.00469(12)	0.00680(15)	0.00553(13)	0.00008(9)	0.00192(9)	0.00025(9)
Mo2	0.00455(12)	0.00743(15)	0.00560(13)	−0.00002(9)	0.00192(9)	−0.00033(9)
Fe1	0.0087(2)	0.0152(3)	0.0084(2)	0.00036(17)	0.00203(19)	−0.00072(17)
S1	0.0068(3)	0.0073(3)	0.0068(3)	−0.0005(3)	0.0023(3)	0.0000(3)
S2	0.0065(3)	0.0071(3)	0.0079(3)	−0.0004(3)	0.0034(3)	0.0004(3)
S3	0.0059(3)	0.0075(3)	0.0076(3)	−0.0005(3)	0.0028(3)	−0.0002(3)
S4	0.0073(3)	0.0069(3)	0.0074(3)	−0.0002(3)	0.0032(3)	−0.0002(3)

Table 6. Selected bond distances (Å) and BVS (bond-valence sum) for ferrodimolybdenite

Atoms	distance	atoms	distance	atoms	distance	Atom	BVS
Mo1–S1	2.3628(9)	Mo2–S1	2.3655(9)	Fe1–S1	2.4247(10)	Mo1	2.87
Mo1–S1	2.3941(9)	Mo2–S4	2.3682(9)	Fe1–S4	2.4440(10)	Mo2	2.86
Mo1–S4	2.4362(9)	Mo2–S4	2.4345(10)	Fe1–S3	2.4869(11)	Fe1	2.32
Mo1–S3	2.4615(9)	Mo2–S3	2.4670(9)	Fe1–S3	2.4915(10)	S1	2.12
Mo1–S2	2.5513(9)	Mo2–S2	2.5646(9)	Fe1–S2	2.5128(11)	S2	1.88
Mo1–S2	2.5653(8)	Mo2–S3	2.5824(9)	Fe1–S2	2.5176(10)	S3	2.08
<Mo1–S>	2.462	<Mo2–S>	2.464	<Fe1–S>	2.480	S4	1.98

BVS calculated using *ECoN21* (Ilinca, 2022) and the bond-valence parameters of Brown and Altermatt (1985).

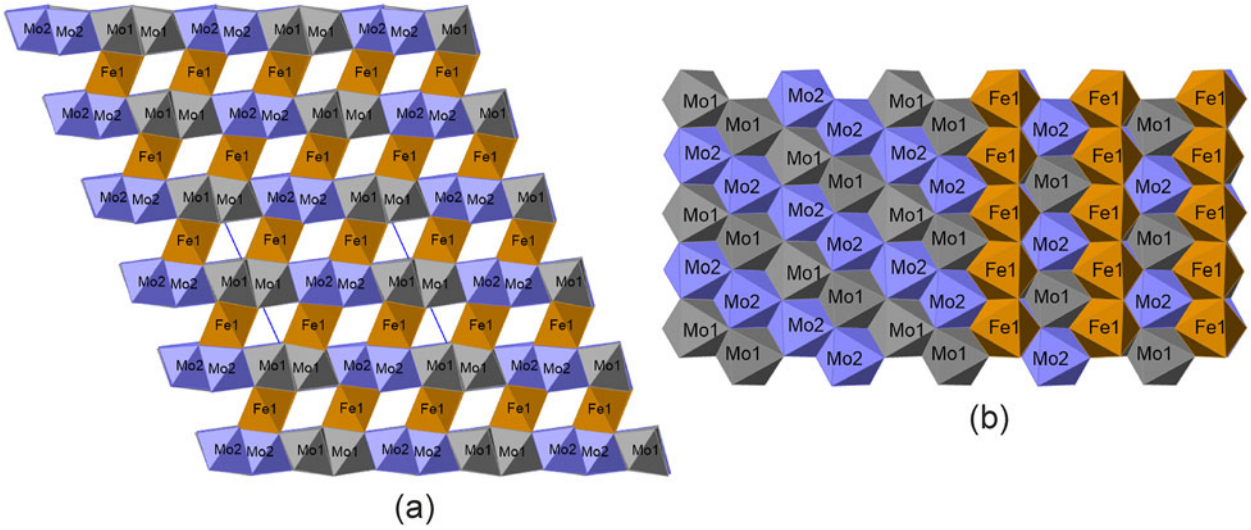

Figure 6. (a) The structure of ferrodimolybdenite (*C*2/*c*) is built up by octahedral layers $(MoS_2)^{1-}$, between which Fe^{2+} cations are located. Projection on (010). (b) Octahedral layers in ferrodimolybdenite are formed by two types of octahedra $(MoS_6)^{9-}$, between which there are columns of Fe-octahedra $(FeO_6)^{10-}$ (only three columns are shown). Drawn using *CrystalMaker 2.7*® software.

Taking into account the systematic absences, it was found that two space groups are possible for ferrodimolybdenite, namely *C*1*c*1 (no. 9) and *C*2/*c* (no.15). Statistical analysis of the intensities of the reflections using the *GRAL* programme implemented in the *CrysAlis*^{Pro} package (Rigaku Oxford Diffraction, 2015) suggests that the space group should be centrosymmetric, i.e. the mean $|E^2 - 1|$ value is equal to 1.202 (expected 0.968 centrosymmetric and 0.736 non-centrosymmetric), suggesting that the space group should be centrosymmetric (Howells *et al.*, 1950; Dolomanov *et al.*, 2009). The refinement of the crystal structures showed that in the space group *C*1*c*1, there were 127 necessary parameters and $R_1 = 0.0332$, whereas in the space group *C*2/*c*, there were 64 necessary parameters and $R_1 = 0.0297$. We believe that the studied crystal of ferrodimolybdenite, which formed at high temperature from sulfide melt at low pressure, has *C*2/*c* symmetry.

Discussion

The melting of a heterogeneous protolith determined the formation of individual metal droplets in the paralava. The metal droplets were saturated with sulfur and phosphorus due the flow of hot reduced gases, which are by-products of combustion processes (Galuskin *et al.*, 2025). A cristobalite fish-scale texture, which appears at the phase transition from cubic to tetragonal cristobalite has been found (Schmieder *et al.*, 2009). The cubic polymorph of cristobalite is stable at high temperature and low pressure and spontaneously transitions to the tetragonal form on cooling (Damby *et al.*, 2014). The detection of the fish-scale texture suggests that the paralava had a temperature above 1400°C (Galuskin *et al.*, 2023a). The sulfide nodule minerals crystallised later than the rock-forming minerals of the paralava. The sulfide melt in the paralava migrated short distances through numerous gas channels in the incompletely crystallised paralava. We believe that karwowskiite, the merrillite-group mineral found at the boundary of this sulfide nodule and the paralava, crystallised in the melt film on the amygdule wall before it was filled with sulfide melt (Galuskin *et al.*, 2024).

Nickelphosphide was one of the first minerals to crystallise in the sulfide melt, forming single crystals (Figs 1b, 2a). Ferrodimolybdenite was also one of the first to form, as it is usually represented by idiomorphic crystals in contact with sulfides or tetrataenite. In one case, an inductive growth surface was observed between a troilite and a ferrodimolybdenite crystal (Fig. 2c), which may indicate their synchronous growth for a certain time interval at a temperature of 1000–1100°C. The crystallisation of ferrodimolybdenite took place under reducing conditions in a monosulfide iron melt, which determined the stabilisation of Mo^{3+} in its structure. Molybdenite (Mo^{4+}) is found in the pentlandite part of the nodule, which is a product of the crystallisation of iron-nickel sulfide melt (Figs 1b, 2a). Crystals of ferrodimolybdenite are located in the troilite part of the differentiated sulfide nodule. A thin layer of pentlandite is often noted between the ferrodimolybdenite crystals and pyrrhotite (Fig. 3c,d). Pentlandite has a non-stoichiometric composition of $(Ni,Fe)_9S_8$, suggesting the

presence of scattered electrons in its structure to compensate for the charge of the cations, and crystallisation from a melt/solution that is an electrolyte. The iron–nickel sulfide melt was the source of electrons that determined the appearance of a mineral with Mo^{3+}, which is unusual in natural systems: $Mo^{4+} + e^{-} = Mo^{3+}$.

Supplementary material. The supplementary material for this article can be found at 10.1180/mgm.2024.82.

Acknowledgements. The authors thank two anonymous reviewers for their remarks and comments that improved an earlier version of the manuscript. Investigations were partially supported by the National Science Centre of Poland Grant No. 2021/41/B/ST10/00130.

Competing interests. The authors declare none.

References

Bentor Y.K. (editor) (1960) Israel. In: *Lexique Stratigraphique International, Asie*, Vol. **III (10.2)**. Centre national de la recherche scientifique, Paris.

Britvin S.N., Murashko M.N., Vapnik Y., Polekhovsky Y.S. and Krivovichev S.V. (2015) Earth's phosphides in Levant and insights into the source of Archean prebiotic phosphorus. *Scientific Reports*, **5**, 8355.

Brown I. and Altermatt D. (1985) Bond-valence parameters obtained from a systematic analysis of the inorganic crystal structure database. *Acta Crystallographica*, **B41**, 244–247.

Canadell E., LeBeuze A., El Khalifa M.A., Chevrel R. and Myung-Hwan Whangbo M.-H. (1988) Origin of metal clustering in transition-metal chalcogenide layers MX2 (M = Nb, Ta, Mo, Re; X = S, Se). *Journal of the American Chemical Society*, **111**, 3778–3782.

Damby D.E., Llewellin E.W., Horwell C.J., Williamson B.J., Najorka J., Cressey G. and Carpenter M. (2014) The α–β phase transition in volcanic cristobalite. *Journal of Applied Crystallography*, **47**, 1205–1215.

Dolomanov O.V., Bourhis L.J., Gildea R.J., Howard J.A.K. and Puschmann H. (2009) OLEX2: A complete structure solution, refinement and analysis program. *Journal of Applied Crystallography*, **42**, 339–341.

Futrzyński J., Juroszek R., Skrzyńska K., Vapnik Y. and Galuskin E. (2023) Uvarovite from reduced native Fe-bearing paralava, Hatrurim Complex, Israel. *Lithosphere*, **2023**. https://doi.org/10.2113/2023/lithosphere_2023_214.

Galuskin E., Galuskina I.O., Kamenetsky V., Vapnik Y., Kusz J. and Zieliński G. (2022) First *in situ* terrestrial osbornite (TiN) in the pyrometamorphic Hatrurim Complex, Israel. *Lithosphere*, **2022**, 8127747.

Galuskin E.V., Stachowicz M., Galuskina I.O., Woźniak K., Vapnik Y., Murashko M.N. and Zieliński G. (2023a) Deynekoite, $Ca_9\square Fe^{3+}(PO_4)_7$ – a new mineral of the merrillite group from phosphide-bearing contact facies of paralava, Hatrurim Complex, Daba-Siwaqa, Jordan. *Mineralogical Magazine*, **87**, 943–954.

Galuskin E.V., Kusz J., Galuskina I.O., Książek M., Vapnik Y. and Zieliński G. (2023b) Discovery of terrestrial andreyivanovite, FeCrP, and the effect of Cr and V substitution on the low-pressure barringerite-allabogdanite transition. *American Mineralogist*, **108**, 1506–1515.

Galuskin E.V., Galuskina I.O., Kusz J., Książek M., Vapnik Y. and Zieliński G. (2024) Karwowskiite, $Ca_9(Fe^{2+}_{0.5}\square_{0.5})Mg(PO_4)_7$—A New Merrillite Group Mineral from Paralava of the Hatrurim Complex, Daba-Siwaqa, Jordan. *Minerals*, **14**, 825. https://doi.org/10.3390/min14080825

Galuskin E., Galuskina I., Vapnik Y., Kusz J., Marciniak-Maliszewska B. and Zieliński G. (2025) Two modes of terrestrial phosphide formation. *American Mineralogist*, **110**, 547–549. https://doi.org/10.2138/am-2024-9315

Galuskina I.O., Vapnik Y., Lazic B., Armbruster T., Murashko M. and Galuskin E.V. (2014) Harmunite $CaFe_2O_4$: A new mineral from the Jabel Harmun, West Bank, Palestinian Autonomy, Israel. *American Mineralogist*, **99**, 965–975.

Galuskina I.O., Galuskin E.V., Pakhomova A.S., Widmer R., Armbruster T., Krüger B., Grew E.S., Vapnik Y., Dzierżanowski P. and Murashko M. (2017) Khesinite, $Ca_4Mg_2Fe_{3+10}O_4[(Fe^{3+}_{10}Si_2)O_{36}]$, a new rhönite-group (sapphirine supergroup) mineral from the Negev Desert, Israel– natural analogue of the SFCA phase. *European Journal of Mineralogy*, **29**, 101–116.

Geller Y.I., Burg A., Halicz L. and Kolodny Y. (2012) System closure during the combustion metamorphic "Mottled Zone" event, Israel. *Chemical Geology*, **334**, 25–36.

Gross S. (1977) The mineralogy of the Hatrurim Formation, Israel. *Geological Survey of Israel Bulletin*, **70**, 1–80.

Guillevic J., Le Marouille J.-Y. and Grandjean D. (1974) Etude structurale de combinaisons sulfurées et séléniées du molybdène. IV. Structures cristallines de $CoMo_2S_4$ et de $FeMo_2S_4$. *Acta Crystallographica*, **B30**, 111–117.

Howells E.R., Phillips D.C. and Rogers D. (1950) The probability distribution of X-ray intensities. II. Experimental investigation and the X-ray detection of centres of symmetry. *Acta Crystallographica*, **3**, 210–214.

Ilinca G. (2022) Charge distribution and bond valence sum analysis of sulfosalts - The ECoN21 Computer Program. *Minerals*, **12**, 924. https://doi.org/10.3390/min12080924.

Khoury H.N., Salameh E.M. and Clark I.D. (2014) Mineralogy and origin of surficial uranium deposits hosted in travertine and calcrete from central Jordan. *Applied Geochemistry*, **43**, 49–65.

Kolodny Y. and Gross S. (1974) Thermal metamorphism by combustion of organic matter: isotopic and petrological evidence. *Journal of Geology*, **82**, 489–506.

Ma C., Beckett J.R. and Rossman G.R. (2014) Allendeite ($Sc_4Zr_3O_{12}$) and hexamolybdenum (Mo,Ru,Fe), two new minerals from an ultrarefractory inclusion from the Allende meteorite. *American Mineralogist*, **99**, 654–666.

Matthews A. and Gross S. (1980) Petrologic evolution of the Mottled Zone (Hatrurim) metamorphic complex of Israel. *Israel Journal of Earth Sciences*, **29**, 93–106.

Murashko M.N., Britvin S.N., Vapnik Y., Polekhovsky Y.S., Shilovskikh V.V., Zaitsev A.N. and Vereshchagin O.S. (2022) Nickolayite, FeMoP, a new natural molybdenum phosphide. *Mineralogical Magazine*, **86**, 749–757.

Novikov I., Vapnik Y. and Safonova I. (2013) Mud volcano origin of the Mottled Zone, South Levant. *Geoscience Frontiers*, **4**, 597–619.

Rigaku Oxford Diffraction (2015) *CrysAlis^{Pro} Software system, version 1.171.38.41q*, Rigaku Corporation, Wroclaw, Poland.

Samy O., Zeng S., Birowosuto M.D. and El Moutaouakil A. (2021). A Review on MoS_2 properties, synthesis, sensing applications and challenges. *Crystals*, **11**, 355. https://doi.org/10.3390/cryst11040355

Schmieder M., Buchner E. and Kröchert J. (2009) "Ballen silica" in impactites and magmatic rocks. *Abstracts 40th Lunar and Planetary Science Conference*. Texas, USA.

Sheldrick G.M. (2015) Crystal structure refinement with *SHELXL*. *Acta Crystallographica*, **C71**, 3–8.

Sokol E., Novikov I., Zateeva S., Vapnik Ye., Shagam R. and Kozmenko O. (2010) Combustion metamorphism in the Nabi Musa dome: new implications for a mud volcanic origin of the Mottled Zone, Dead Sea area. *Basin Research*, **22**, 414–438.

Vapnik Y., Sharygin V.V., Sokol E.V. and Shagam R. (2007) Paralavas in a combustion metamorphic complex: Hatrurim Basin, Israel. *Reviews in Engineering Geology*, **18**, 1–21.

Vaqueiro P., Kosidowski M.L. and Powell A.V. (2002) Structural distortions of the metal dichalcogenide units in AMo_2S_4 (A = V, Cr, Fe, Co) and magnetic and electrical properties. *Chemistry of Materials*, **14**, 1201–1209.

Warr L.N. (2021) IMA–CNMNC approved mineral symbols. *Mineralogical Magazine*, **85**, 291–320.